bioengineering

MDPI

Article

Lipid–Polymer Nanoparticles (LiPoNs) Mediated Codelivery of AntimiR-21 and Gadolinium Chelate in Triple Negative Breast Cancer Theranostics

Felicia Roffo [1,2], Francesca Maria Orlandella [3,4], Neila Luciano [3,4], Giuliana Salvatore [3,4] and Enza Torino [1,2,5,*]

[1] Department of Chemical, Materials and Production Engineering (DICMaPI), University of Naples Federico II, P.le Tecchio 80, 80125 Naples, Italy; felicia.roffo@unina.it
[2] Interdisciplinary Research Center on Biomaterials (CRIB), University of Naples Federico II, P.le Tecchio 80, 80125 Naples, Italy
[3] Department of Medical, Human Movement and Well-Being Sciences, University of Naples Parthenope, 80133 Naples, Italy; francescamaria.orlandella@uniparthenope.it (F.M.O.); neilaluciano14@gmail.com (N.L.); giuliana.salvatore@uniparthenope.it (G.S.)
[4] CEINGE-Biotecnologie Avanzate "Franco Salvatore", 80145 Naples, Italy
[5] Center for Advanced Biomaterials for Healthcare (CABHC), Fondazione Istituto Italiano di Tecnologia, IIT@CABHC, Largo Barsanti e Matteucci 53, 80125 Naples, Italy
* Correspondence: enza.torino@unina.it

Abstract

RNA-based interventions are particularly promising for next-generation therapeutic strategies and hold significant potential when integrated with diagnostic modalities. Among noncoding RNAs, microRNAs (miRNAs) regulate gene expression post-transcriptionally and represent compelling targets for cancer therapy. However, their clinical translation remains hindered by instability, off-target effects, and limited delivery efficiency. Here, we report the microfluidic synthesis of hybrid lipid–polymer nanoparticles (LiPoNs) that co-deliver an AntimiR-21 and the magnetic resonance imaging contrast agent gadolinium diethylenetriamine penta-acetic acid (Gd-DTPA). The LiPoNs were obtained using coupled Hydrodynamic Flow Focusing (cHFF), enabling precise control over lipid–polymer self-assembly and surpassing the compositional limitations reported with conventional micromixers. The resulting AntimiR-21–Gd-DTPA–LiPoNs exhibited an average hydrodynamic diameter of 124 nm, narrow polydispersity (PDI < 0.2), and encapsulation efficiency up to 60%. In MDA-MB-231 breast cancer cells, treatment with AntimiR-21–LiPoNs induced suppression of miR-21 and a corresponding decrease in migratory capacity, demonstrating effective functional delivery and gene expression modulation. These findings establish a versatile microfluidic platform for engineering multifunctional lipid–polymer nanostructures whose hybrid architecture combines the biocompatibility and membrane fusion capability of lipids with the structural robustness and controlled release properties of polymers, thereby advancing RNA-based theranostic design for precision oncology and related applications.

Keywords: microRNA; chitosan; hybrid lipid–polymer nanoparticles

Academic Editors: Huiyi Liang and Tianqi Nie

Received: 7 January 2026
Revised: 2 February 2026
Accepted: 4 February 2026
Published: 12 February 2026

1. Introduction

The nanomedicine community conducts fundamental and technical research on lipid nanoparticles (LNPs) to investigate and optimize their synthetic and biological identity, allowing for the development of promising therapies at a remarkable speed [1,2]. The use

of LNPs is currently under investigation in two main fields: for the delivery of nucleic acids [1–3] and the engineering of cells [4,5]. Their contribution to the delivery is well-known due to the use of modern mRNA COVID-19 vaccines [6,7], while engineering of cells, such as CAR T cells, is spreading fast [8,9].

Among the classes of nucleic acids, mRNAs are more studied for vaccine applications [10], while both siRNA and miRNA make a contribution in targeting and addressing undruggable proteins in the field of cancer treatment [11–13].

Despite their selectivity and specificity [14], only a small number of miRNA-based drugs have entered clinical trials, and none have reached Phase III [15,16], due to their instability, toxicity, adverse effects, and low therapeutic efficacy [17]. Indeed, miRNAs have a short half-life and poor stability in systemic circulation caused by the presence of nuclease in the bloodstream [18]. Other concerns are related to the undesired off-target effects and their uncontrolled activation of innate immune responses [19,20]. Moreover, at the cellular level, naked miRNAs are partially internalized by cells and are prone to degradation in endosomal/lysosomal vesicles [18–20].

To face these hurdles, bioengineering has exploited the material properties of lipids or polymers in the form of nanoparticles individually [19–22]. Despite the frequent use and versatility of pure lipid-based NPs (LNPs), their self-assembly behavior makes them less stable in biological environments, compromising their prolonged encapsulation capability. Different types of polymer materials, especially positively charged polyplexes, widely studied for nucleic acid release in the cytoplasm, suffer from toxicity and slow and poor biodegradability [19,20,23,24].

In this framework, the combination of lipid and polymer materials to obtain hybrid lipid–polymer or lipid–hydrogel nanoparticles takes the advantageous properties of both classes of materials and leads nanotechnologies to deliver biologics properly, overcoming limitations of systems based only on a single type of material, such as lipids or polymers and polymer–hydrogels [25–34]. Indeed, this combination of materials potentially confers to the nanocarriers the capability of co-entrapping multiple agents of different chemical nature, also to be applied in theranostics [26]. In detail, in lipid–polymer hybrid systems for RNA delivery, the polymer or polymer hydrogel component plays a non-ancillary but structurally and functionally determinative role. Beyond serving as a passive scaffold, the polymer/hydrogel matrix contributes to mechanical stabilization, controlled spatial confinement, and temporal regulation of RNA release, thereby complementing the transfection efficiency typically associated with lipid-based carriers. The properties of the polymeric network modulate diffusion kinetics, protect RNA cargo from premature degradation, and enable sustained or stimuli-responsive release profiles that are difficult to achieve with lipid nanoparticles alone. Within this hybrid architecture, lipids primarily facilitate cellular uptake and endosomal escape, while the polymer or polymer-hydrogel core governs macroscopic handling, residence time, and dose control, resulting in a synergistic system in which transport efficiency and delivery precision are decoupled yet harmonized. Finally, in the delivery of diagnostic molecules and therapeutic drugs, polymer features allow the tuning of release mechanisms and preserve the boosted diffusion, while peculiar biomimetic properties of lipids mediate different cellular and intracellular pathways, such as fusion mechanisms [35–37].

Particularly for nucleic acids, several combined lipid–hydrogel architectures have been proposed where mRNA is absorbed on the lipid surface via electrostatic interactions for mRNA vaccines. Among them, Su et al. [38] developed a pH-responsive poly (β-amino ester) (PBAE) core covered by a phospholipid shell. Yang et al. [39] employed a hybrid nanovaccine consisting of a poly lactic-co-glycolic acid (PLGA) core that entrapped the toll-like receptor TLR7 adjuvant coated by the lipid shell. Recently, Kliesch

et al. [40] examined the impact of different amounts of lipids, keeping the PLGA polymer component constant, on the stability, compatibility, and delivery efficacy of hybrid NPs in dendritic cells. Regarding the entrapment of RNAs in the polymer core, Huang et al. [41] presented miR-29 b-loaded transferrin-conjugated nanoparticles, where the microRNA was loaded in the polyethyleneimine (PEI) polymer coated with a mixture of lipids (1,2-dioleoyl-sn-glycero-3-phosphoethanolamine DOPE/linoleic acid/1,2-dimyristoyl-sn-glycerol, methoxy polyethylene glycol DMG-PEG) and transferrin (Tf) conjugated distearoyl phosphatidylethanolamine-polyethylene glycol Tf-PEG-DSPE, for the treatment of acute myeloid leukemia. Shi et al. [42] developed a hybrid system made up of an aqueous core containing the siRNA stabilized by the positively charged lipid-like compound G0-C14, covered by a hydrophobic PLGA polymer shell and lipid–PEG. Küçüktürkmen et al. [43] studied the hybrid lipid–polymer NPs, made up of PLGA, polycaprolactone (PCL), and lipid, for the co-delivery of pemetrexed and AntimiR-21 in glioblastoma cells, showing exceptional accumulation in the nucleus of U-87 MG cells. Regarding the use of hybrid NPs for multimodal imaging and therapeutic purposes, Tng et al. [26] developed stratified NPs, where the PLGA core loads the rhodamine 6G dye, the outer lipid layer entraps the paclitaxel, and on the surface, it is attached to the gadolinium chelates. More recently, Ottonelli et al. highlighted the advantages and challenges of polymer–lipid hybrid nanoparticles for the delivery of biological drugs [28].

These hybrid NPs were generally produced by traditional techniques based on emulsification, solvent evaporation, and film hydration methodologies, which do not guarantee a high level of control and reproducibility of the properties [19,44]. Indeed, the conventional batch techniques have been superseded by alternative approaches to control the multicomponent features and overcome processing issues such as high temperatures, extreme acid or basic conditions, solvent solubility, and post-production steps that pose a challenge to preserving miRNAs [19,44]. In the last decade, microfluidics has taken an essential role in the development of NPs for the loading of RNA-based drugs by exploiting different transport mechanisms of species and a variety of device geometries, allowing the reduction in the potential risk for RNA degradation and obtaining particles with tunable features, controlled size distribution, high-loading, and co-loading ability of different compounds [44–47]. The potential of microfluidics has already been exploited to entrap large biomolecules such as mRNA [48,49], DNA [48,50] and siRNA [48,51,52], and imaging molecules [53–56]. Indeed, Zhao et al. [57] evaluated the effect of the addition of different polymer materials to a combination of N^1,N^3,N^5-tris(2-aminoethyl) benzene-1,3,5 tri-carboxamide (TT), DOPE, cholesterol, and DMG-PEG_{2000} in a microfluidic process to improve the delivery of mRNA. Then, Meyer et al. [58] exploited the microfluidic technology for producing lipid–polymer NPs, made up of PLGA and lipid mixture, which entrapped or absorbed mRNA. A toroidal micromixer was employed to produce lipid–polymer hybrid NPs for the loading of pDNA [59]. Furthermore, Wei et al. [60] developed a three-stage microfluidic-based holonomic constraints device for the production of siRNA-loaded lipid/polymer NPs (lipid/PCL-PEI/siRNA NPs), reporting interesting in vitro and in vivo results on the downregulation of EGFR mRNA and the protein expression.

Recently, Alawi et al. [61] explored the potential of lipid–polymer hybrid nanoparticles as a next-generation drug delivery system for breast cancer therapy, and recently, we proposed a novel one-step microfluidic approach to guide polymer–lipid interactions by the coupled Hydrodynamic Flow Focusing (cHFF) [55] for the production of lipid–polymeric hybrid nanoparticles (LiPoNs). In this work, we proved that the same system can be applied to co-entrap nucleic acid, Antisense miR-21 (AntimiR-21), and Gd-DTPA for theranostics of triple-negative breast cancer.

LiPoNs through cHFF [55] were finely tuned to obtain lipid–hydrogel nanoparticles made of a chitosan core and lipid bilayer, more precisely to control the interaction, at the low pH, of the protonated amine groups of the chitosan and negatively charged nucleic acids, leading to the formation of a stable polyelectrolyte complex. Using AntimiR-21 as a model RNA-drug, we validated in MDA-MB-231 human breast cancer cells the biological ability of AntimiR-21-loaded LiPoNs to act as a nanomedicine tool to inhibit the miRNA expression and act on cell migration. Simultaneously, the relaxivity properties of the system were also investigated.

2. Materials and Methods

2.1. Materials

L-α-phosphatidylcholine from soybean (SPC; lyophilized powder, purity ≥ 99%, Mw ≈ 776 g/mol; stored at −20 °C), cholesterol (Chol; powder, purity ≥ 99%, Mw = 386.65 g/mol, empirical formula $C_{27}H_{46}O$; stored at −20 °C), and chitosan (CH; low molecular weight, 50,000–190,000 Da; soluble in dilute aqueous acid) were used as received. Additional reagents included sodium hydroxide (NaOH; pellets, ACS reagent grade, 97.0%, Mw = 40.00 g/mol) and gadolinium (III) diethylenetriaminepentaacetic acid di-hydrogen salt hydrate (Gd-DTPA; 97.0%, Mw = 547.57 g/mol). All these materials were purchased from Sigma-Aldrich (St. Louis, MO, USA). Antisense miR-21 (AntimiR-21; sequence 5′-UCAACAUCAGUCUGAUAAGCUA-3′; DESALT purification) was obtained from Sigma-Aldrich (St. Louis, MO, USA).

Solvents comprised glacial acetic acid (AcOH; ≥99.8%, Mw = 60.05 g/mol, CH_3COOH; ROMIL Pure Chemistry, Cambridge, UK), absolute anhydrous ethanol (EtOH; ≥99.9%, Mw = 46 g/mol, C_2H_5OH; Carlo Erba Reagents, Cornaredo, Italy), and filtered Milli-Q water (Milli-Q Plus, Q-POD®, Merck KGaA, Darmstadt, Germany). Phosphate-buffered saline (PBS, tablet form) used for dialysis was also purchased from Sigma-Aldrich.

The human epithelial breast cancer cell line MDA-MB-231 was obtained from the Leibniz Institute DSMZ–Deutsche Sammlung von Mikroorganismen und Zellkulturen GmbH (Braunschweig, Germany). Cells were cultured in Dulbecco's Modified Eagle Medium (DMEM, high glucose; Sigma-Aldrich) supplemented with 4.5 g/L glucose, 10% (*v*/*v*) fetal bovine serum (FBS; Sigma-Aldrich), 2 mM L-glutamine, and 1% (*v*/*v*) antibiotic solution (Thermo Fisher Scientific). Cell cultures were maintained at 37 °C in a humidified atmosphere containing 5% CO_2 and harvested using trypsin–EDTA.

Dimethyl sulfoxide (DMSO; molecular biology grade), thiazolyl blue tetrazolium bromide (MTT; soybean-derived, 98%), and Lipofectamine 3000 transfection reagent (Cat. No. L3000008) were obtained from Thermo Fisher Scientific (USA).

2.2. Microfluidic Set-Up for Coupled Hydrodynamic Flow-Focusing Approach (cHFF)

A microfluidic setup to produce the LiPoNs has already been published [55]. In brief, a quartz microfluidic chip (22.5 mm × 15 mm × 4 mm; Dolomite Center Ltd., Royston, UK) featuring five parallel inlet channels converging at a 45° junction into a single outlet was used in this study. Glass syringes with volumes ranging from 2.5 to 10 mL (CETONI GmbH, Thuringia, Germany) were connected to the chip via FEP tubing (1/16″ × 0.25 mm and 0.8 × 0.25 mm) and driven by a low-pressure syringe pump (neMESYS 290N, CETONI GmbH, Germany). Two-way in-line ETFE valves were positioned between the syringes and the microfluidic device to allow automated loading and continuous reagent delivery. The outlet flow was collected through FEP tubing (0.8 × 0.25 mm) into glass vials containing water. Flow-focusing behavior within the microchannels was observed using an optical fluorescence microscope (Olympus IX71, Olympus Italia srl, Segrate, MI, Italy) equipped with a 4× scanning objective.

2.3. AntimiR-21 Behavior in CH-AcOH–Water Ternary System

The stability of AntimiR-21 under different environmental conditions was evaluated experimentally. As a control, an aqueous solution of AntimiR-21 (26 μg/mL) was compared with buffer solutions containing the same concentration of AntimiR-21 incubated either at room temperature or at 4 °C. Additional experiments were conducted at acidic pH values (2.6 and 4.3). These buffer conditions were obtained by adding 0.5% (*v*/*v*) acetic acid (AcOH) to water, with or without 25 mM NaOH, respectively. Separate aliquots of AntimiR-21 were prepared for each condition, and RNA degradation over time (1–4 h) was monitored using a Multiskan SkyHigh Microplate Spectrophotometer (Thermo Fisher Scientific). RNA concentration was quantified at λ = 260 nm with a μDrop Plate.

Subsequently, AntimiR-21 stability was tested in conditions mimicking those used for microfluidic encapsulation. Specifically, AntimiR-21 (54 μg/mL) was dispersed in a chitosan solution (0.01% *w/v* in 1% *v/v* AcOH), with or without gadolinium diethylenetriamine penta-acetic acid (Gd-DTPA; 0.4% *w*/*v*). For both formulations, the pH was adjusted to ~4 with 50 mM NaOH. RNA stability was expressed as the percentage of RNA concentration measured after treatment relative to the untreated AntimiR-21 control solution.

2.4. Formulations of AntimiR-21-Loaded LiPoNs

Coupled Hydrodynamic Flow Focusing (cHFF) [55] was employed to produce lipid–polymer nanoparticles (LiPoNs), including AntimiR-21-loaded LiPoNs (AntimiR-21–LiPoNs) and co-loaded AntimiR-21/Gd-DTPA–LiPoNs. The organic phase consisted of an ethanol–water mixture (65:35 *v*/*v*) containing 0.0072% (*w*/*v*) lipids (soy phosphatidylcholine/cholesterol, SPC/Chol, 8:1 mass ratio), stirred overnight before injection through the side channels. The aqueous phase was prepared as 0.01% (*w*/*v*) chitosan (CH) dissolved in 1% (*v*/*v*) acetic acid (AcOH), stirred for at least 1 h, and adjusted to pH ≈ 4 with 50 mM NaOH.

For AntimiR-21–LiPoNs, AntimiR-21 (11 μM) was added to the polymer solution and stirred for 10 min prior to injection into the middle channel. For AntimiR-21/Gd-DTPA–LiPoNs, Gd-DTPA (0.4% *w*/*v*) was added to the same polymer–RNA solution. Microfluidic assembly was performed at a flow rate ratio (FR^2) of 0.073, defined as the flow rate of the middle channel (3 μL/min) relative to the side channel (41 μL/min), for a total processing time of 80 min.

The resulting nanoparticles were collected in 7 mL of pure water and stirred for 40 min at 25 °C. Purification was carried out by mild solvent-gradient dialysis against PBS diluted 1:1 with water, using a Spectra-Por Float-A-Lyzer G2 (MWCO 25–50 kDa; Sigma-Aldrich, St. Louis, MO, USA). Samples were dialyzed at a sample-to-buffer ratio of 1:3 under continuous stirring for 1 h at room temperature.

2.5. In Vitro MRI Relaxation Time Measurement

Changes in longitudinal relaxation time (T_1) were assessed at 1.5 Tesla and 37 °C using a Minispec Bench-Top Relaxometer (Bruker Corporation, Billerica, MA, USA). For each measurement, 300 μL of sample was placed in a glass tube, and nanoparticles were analyzed both undiluted and diluted 1:1 in water. The Free Induction Decay (FID) sequence was applied to optimize gain settings and prevent signal saturation. T_1 values were determined using saturation recovery and inversion recovery pulse sequences, while relaxation time distributions were calculated using the CONTIN algorithm.

2.6. Synthetic Identity of AntimiR-21-Gd-DTPA-LipoNs

The hydrodynamic diameter and particle concentration of the nanoparticles were measured by nanoparticle tracking analysis (NTA) using a NanoSight NS300 system (Malvern

Instruments Ltd., Malvern, UK; NTA software v3.4, sCMOS camera, 488 nm blue laser) at room temperature (Figure S2). Particle size distribution and concentration are reported as the mean from three independent measurements.

The ζ-potential was determined at 25 °C using a Zetasizer Nano ZS (Malvern Panalytical, UK) operating in monomodal analysis mode. Measurements were performed by loading 1 mL of nanoparticle suspension into a folded capillary ζ-potential cell (Malvern Panalytical, UK).

Morphological characterization was carried out using both field emission scanning electron microscopy (FE-SEM; UltraPlus Field Emission, Carl Zeiss, Oberkochen, Germany) and transmission electron microscopy (TEM; FEI, Hillsboro, OR, USA). For the transmission electron microscope (TEM) analysis, 8 µL of nanoparticle suspension was deposited onto Formvar/carbon-coated 200-mesh copper grids (Agar Scientific Ltd., Stansted, UK), air-dried overnight, and directly imaged. The same grids were subsequently examined by FE-SEM after sputter-coating with a 5 nm gold layer.

The encapsulation efficiency (EE%) of Gd-DTPA was determined by comparison with calibration curves prepared in water (0–100 µM; Figure S3). AntimiR-21 encapsulation was quantified using a Multiskan SkyHigh microplate spectrophotometer (Thermo Fisher Scientific, Waltham, MA, USA), using unloaded LiPoNs as background. The EE% of both AntimiR-21 and Gd-DTPA was calculated according to the following equation:

$$EE\% = \frac{CM}{CT} \times 100$$

where C_M is the experimentally measured concentration in the nanoparticle suspension, and C_T is the theoretical input concentration of AntimiR-21 or Gd-DTPA used in the microfluidic process.

The Qubit microRNA Assay Kit (Thermo Fisher Scientific) was used for the quantification of microRNAs using the Qubit 4 fluorometer (Thermo Fisher Scientific).

2.7. RNA Extraction and q-RT-PCR

Total RNA was purified from MDA-MB-231 cells 72 h post-transfection using TRIzol reagent (Thermo Fisher Scientific, Cat. No. 15596026). RNA concentrations were quantified with a Qubit 4 fluorometer (Thermo Fisher Scientific). For miR-21 detection, 100 ng of total RNA was reverse-transcribed using the miRCURY LNA RT Kit (Qiagen, Limburg, The Netherlands, Cat. No. 339340). Quantitative PCR was performed with SYBR® green–based detection (Qiagen, Cat. No. 339371) and the miRCURY LNA miRNA probe assay specific for miR-21 (Qiagen, Cat. No. 339350; GeneGlobe ID: ZP00000445). Data was normalized against the endogenous control U6 snRNA (Qiagen; GeneGlobe ID: ZP00030496).

For the detection of miR-21 target genes (PTEN and PDCD4), 1 µg of total RNA was reverse-transcribed using the SuperScript™ III First-Strand Synthesis SuperMix Kit (Thermo Fisher Scientific, Cat. No. 18080400), following the manufacturer's instructions. qRT-PCR was performed with iQ SYBR Green Supermix (Bio-Rad, Cat. No. 1708882) on a C1000 Touch thermal cycler (Bio-Rad). Data acquisition and analysis were carried out using CFX Maestro software version 1.0 (Bio-Rad). Gene expression levels were calculated with the ΔΔCt method, using β-actin as the endogenous control. All experiments were performed in triplicate across three independent biological replicates. Oligonucleotide sequences used for RT–qPCR are reported in Table S1.

2.8. Western Blot Analysis

MDA-MB-231 cells were seeded in 6-well plates and treated for 72 h with 33 nM AntimiR-21 delivered via lipid–polymer nanoparticles (LiPoNs). Since this study is specif-

ically focused on evaluating the role of the hybrid LiPoNs architecture in RNA-based drug delivery, and AntimiR-21 sequence-dependent biological effects have already been proven, a scrambled RNA sequence was not employed as a control. Following treatment, total proteins were extracted as previously described [62]. Equal amounts of protein were resolved on 12.5% SDS–polyacrylamide gels and transferred to nitrocellulose membranes. Membranes were blocked with 5% (*w*/*v*) non-fat dry milk in TBS-T and incubated overnight at 4 °C with the following primary antibodies: anti-PTEN (1:1000, Cat. No. 138G6, Cell Signaling Technology, Danvers, MA, USA), anti-PDCD4 (1:1000, Cat. No. D29C6, Cell Signaling Technology), and anti-α-tubulin (1:10,000, Cat. No. T9026, Merck KGaA, Darmstadt, Germany). After washing, membranes were incubated with HRP-conjugated secondary antibodies for 1 h at room temperature. Protein bands were visualized using an enhanced chemiluminescence (ECL) detection reagent (Thermo Fisher Scientific) and imaged on a ChemiDoc system (Bio-Rad, Hercules, CA, USA).

2.9. Wound Healing Assay

To assess the migratory capacity of breast cancer cells following miR-21 silencing, a wound healing assay was performed. In brief, 1×10^5 MDA-MB-231 cells were seeded in 12-well plates and treated the following day with AntimiR-21–LiPoNs, empty LiPoNs, or AntimiR-21 delivered via Lipofectamine 3000. After 48 h, a scratch was introduced into the cell monolayer using a pipette tip, and cell migration into the wound area was monitored by automated time-lapse microscopy (Celldiscoverer 7, Zeiss, Munich, Germany) under incubator-controlled conditions. Images were captured at 100× magnification every 2 h across three independent fields per well. Wound areas were quantified using ZEN 3.0 software (Zeiss), and migration capacity was expressed as the percentage of wound closure over time.

2.10. Cell Viability

Cytotoxicity was assessed using the MTT assay. MDA-MB-231 cells were seeded at a density of 1×10^4 cells per well in 96-well plates and allowed to adhere for 24 h prior to treatment. Cells were then incubated with fresh medium containing either AntimiR-21 delivered with Lipofectamine 3000, AntimiR-21–LiPoNs, or AntimiR-21–Gd-DTPA–LiPoNs (final concentrations: AntimiR-21, 33 nM; lipids, 12 μg/mL; Gd-DTPA, 28 μM). Empty LiPoNs and Gd-DTPA–LiPoNs were also tested at equivalent concentrations. Treatments were carried out for 24 and 48 h.

At the end of each incubation period, the medium was removed, cells were washed with PBS, and fresh medium containing MTT (0.5 mg/mL, 0.22 μm filtered) was added. After 3 h of incubation, the medium was discarded, and the resulting formazan crystals were dissolved in 200 μL of DMSO. Plates were incubated for 30 min to ensure complete solubilization, and absorbance was measured at 556 nm in triplicate using a Multiplate Reader Photometer (EnSpire, PerkinElmer Inc., Waltham, MA, USA). Cell viability was expressed as a percentage relative to untreated control cells.

$$\text{Cell viability \%} = \frac{\text{AU of Cells tested AntimiR} - 21 \text{ formualtions}}{\text{AU of Untreated Control Cells}} \times 100 \quad (1)$$

where the AU is the measured absorbance in triplicate.

2.11. Statistical Analysis

Data were analyzed using GraphPad Prism 9 (GraphPad Software, La Jolla, CA, USA). Results are presented as mean ± standard error of the mean. Statistical significance was assessed using two-tailed unpaired Student's *t*-tests, with $p < 0.05$ considered significant.

.

3. Results

3.1. Optimization of Coupled Hydrodynamic Flow Focusing (cHFF) to Produce AntimiR-21 Gd-DTPA Lipid–Polymer NPs

Here, we propose the encapsulation by coupled Hydrodynamic Flow Focusing (cHFF) of miRNA in hybrid polymer–lipid nanoparticles (LiPoNs) (Figure 1) [55].

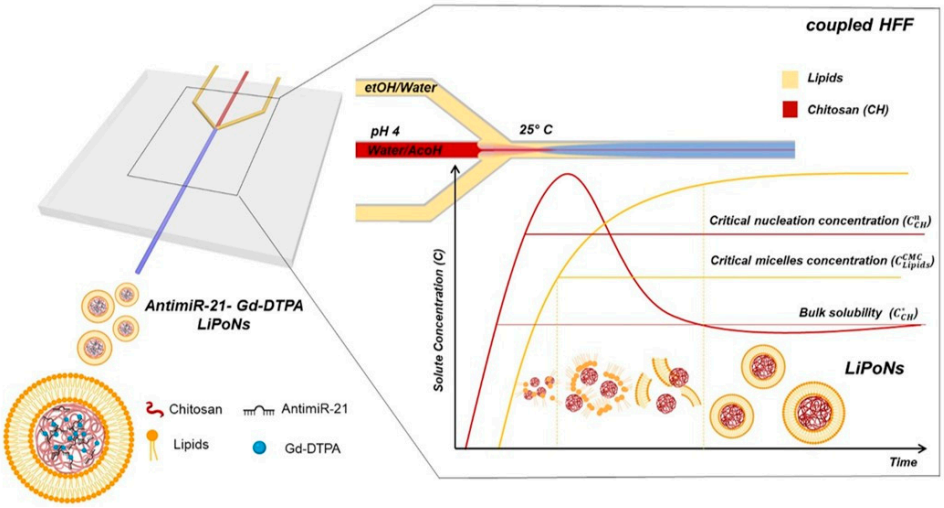

Figure 1. Coupled Hydrodynamic Flow Focusing (cHFF) to produce AntimiR-21-Gd-DTPA-lipid–polymer nanoparticles (LiPoNs). Schematic representation of the cHFF strategy and the LiPoNs structure (**left**). Schematic illustration of nanoprecipitation and self-assembly processes implemented in microfluidics for LiPoNs production (**right**). Some graphic elements of nanostructures in Figure 1 were created using BioRender.com.

A schematic illustration of the cHFF process implemented in microfluidics for the production of AntimiR-21-LiPoNs is reported in Figure 1 (left), where the chitosan (0.01% w/v) in acid solution (AcOH-NaOH/1% v/v-50 mM) containing the AntimiR-21 (11 µM) is sheeted by two side streams of lipids (0.0072% w/v, 8:1 mass ratio SPC:Chol) dissolved in an etOH-water (65–35% v/v) mixture. The Gd-DTPA compound was added to the middle solution (0.4% w/v) to produce the co-loaded AntimiR-21-Gd-DTPA-LiPoNs. The microfluidic cHFF process is conducted by setting the side flow rate at 41 µL/min, while the middle one is at 3 µL/min for a flow rate ratio (FR^2) of 0.073.

Starting from the previous results on cHFF [55], we adjusted the microfluidic process to take advantage of the mutual diffusion of solvents to promote the nucleation of chitosan, its complexation with the AntimiR-21, the formation of the lipid bilayer fragments, and simultaneously their coupling; see Figure 1 (right).

To avoid damaging AntimiR-21, we performed a preliminary bulk study to assess its chemical stability in the form of degradation under cHFF process conditions, referring to the central injection channel. In particular, we evaluated in bulk the effect of the exogenous parameters [63], such as changes in temperature, pH, and material concentration, to optimize the cHFF process for AntimiR-21-LiPoNs (Figure S1). Following the studies reported on AntimiR-21 chemical stability (Figure S1a–d) in terms of degradation, all the experiments for the obtaining of the AntimiR-21-LiPoNs were conducted by dissolving for 10 min the AntimiR-21 in the polymer solution at pH ~ 4 before being injected in the central channel of the microfluidic device, where the cHFF process was carried out at room temperature.

The nanoparticles were analyzed in terms of the mean and mode of NP size, standard deviation (SD) value, and zeta potential, obtained by NanoSight NTA and Zetasizer Nano (Figures 2 and S2, Table 1).

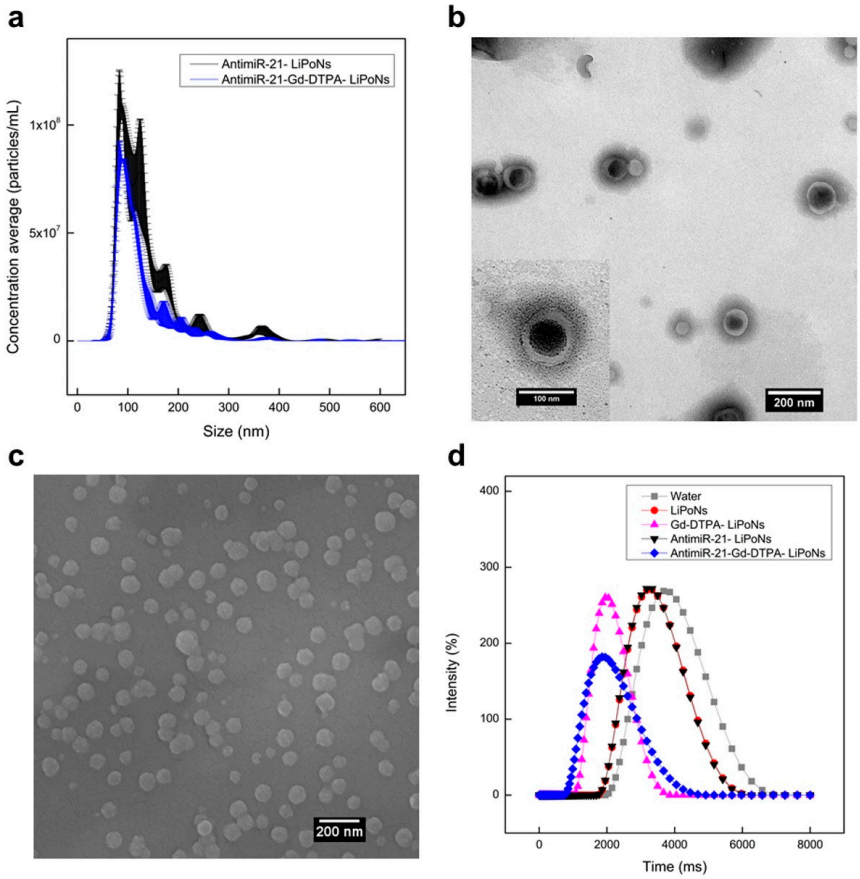

Figure 2. LiPoNs morphological characterization and relaxation time measurement. (**a**) Size distribution of AntimiR-21-LiPoNs (black) and AntimiR-21-Gd-DTPA-LiPoNs (blue) as a function of the mean nanoparticle concentration from the three measurements. (**b**) TEM and (**c**) FE-SEM of AntimiR-21-LiPoNs. (**d**) Comparison of longitudinal relaxation time distributions of water, LiPoNs, Gd-DTPA-LiPoNs, AntimiR-21-LiPoNs, and AntimiR-21-Gd-DTPA-LipoNs.

Table 1. Table summary of nanoparticles mean size, mode, standard deviation (SD), zeta potential, and concentration of different LiPoNs formulations.

	Mean Size ± St. Error (nm)	**Mode ± St. Error (nm)**	**SD ± St. Error (nm)**	**Zeta Potential ± St. Error (mV)**	**Concentration (particles/mL)**
LiPoNs	155 ± 0.8	104 ± 4.9	84.8 ± 1.5	−13.3 ± 1.0	1.17×10^{10}
Gd-DTPA-LiPoNs	149 ± 2.6	107.6 ± 6.1	81.0 ± 3.7	−9.2 ± 1.1	5.92×10^{9}
AntimiR-21-LiPoNs	134 ± 2.1	87.9 ± 2.8	68.7 ± 1.3	−8.7 ± 0.5	7.91×10^{9}
AntimiR-21-Gd-DTPA-LiPoNs	124 ± 3.2	88.5 ± 3.7	62.4 ± 6.1	−13.3 ± 0.5	5.09×10^{9}

The direct and real-time visualization of AntimiR-21-LiPoNs by NTA (Figures 2 and S2) reports a monodisperse population of NPs, confirming the high-resolution particle distribution (Figure 2a), showing a peak at 134 nm with 90% of the particles being 201 nm. The mean size value of AntimiR-21-LipoNs (7.91×10^9 particles/mL) correlates with the transmission and scanning electron images, TEM and FE-SEM, respectively, reported in Figure 2b,c. A recognizable dark core within a lipid bilayer vesicle is shown in the TEM image, Figure 2b. The clear resolution of the lipid bilayer can be associated with the enhanced electron contrast due to the AntimiR-21 located in the chitosan core of LiPoNs.

The longitudinal relaxation time distributions of AntimiR-21-Gd-DTPA-LiPoNs (T1 = 1830 ms) in Figure 2d confirm the loading of Gd-DTPA contrast agent (EE-62%)

within the LiPoNs nanostructures, which does not affect the size of the LiPoNs, as shown in Figure 2a and Table 1. Furthermore, the zeta potential data show a slight increase in the negative charge from −8.7 mV to −13.3 mV for AntimiR-21 and AntimiR-21-Gd-DTPA-LipoNs, respectively.

3.2. Silencing by AntimiR-21-Loaded LiPoNs

As reported by The Cancer Genome Atlas (TCGA) Breast Cancer (BRCA) database, high miR-21 expression is correlated with a reduction in the overall survival ratio of patients under study [64,65], and extensive studies show its involvement in tumor pathogenesis. MDA-MB-231, a human epithelial triple-negative breast cancer cell line, expresses significant miR-21 levels with respect to other breast cancer cell lines (MCF-7 and SKBR3 cells) [65]. Therefore, the inhibition of miR-21, achieved with Antisense miRNA, consists of a single-stranded oligonucleotide with a complementary sequence to the mature miRNA [66] and can inhibit its role in carcinogenesis. To test the effects of AntimiR-21-LiPoNs in MDA-MB-231 cells, we analyzed the resulting expression of miR-21, its targets, and the underlying biological effects. The MDA-MB-231 cells were treated with AntimiR-21-LiPoNs, free AntimiR-21, and LiPoNs for 72 h; the total RNA was extracted from the cells, and the miR-21 expression level was quantified by q-RT-PCR. The cells treated with LiPoNs were used as a control (equal to 1). A reduction in miR-21 expression from 1 to 0.08 is reported for the cells treated with 33 nM of AntimiR-21-LiPoNs (Figure 3a). This reduction in miR-21 expression using NPs formulation follows the previously reported cellular uptake of NPs encapsulated miRNAs due to the shielding of miRNA charge groups [19,66]. In parallel, a comparison between the commercially available transfection agent, the Lipofectamine 3000 (Lipo), and the newly designed hybrid vector, LiPoNs, was conducted, performing the same experiment at 72 h. Upon 72 h of treatment with AntimiR-21 Lipofectamine-mediated transfection (Lipo + AntimiR-21), the cells show a miR-21 downregulation from 1 to 0.26 (Figure 3b), less effective than that obtained by delivering LiPoNs.

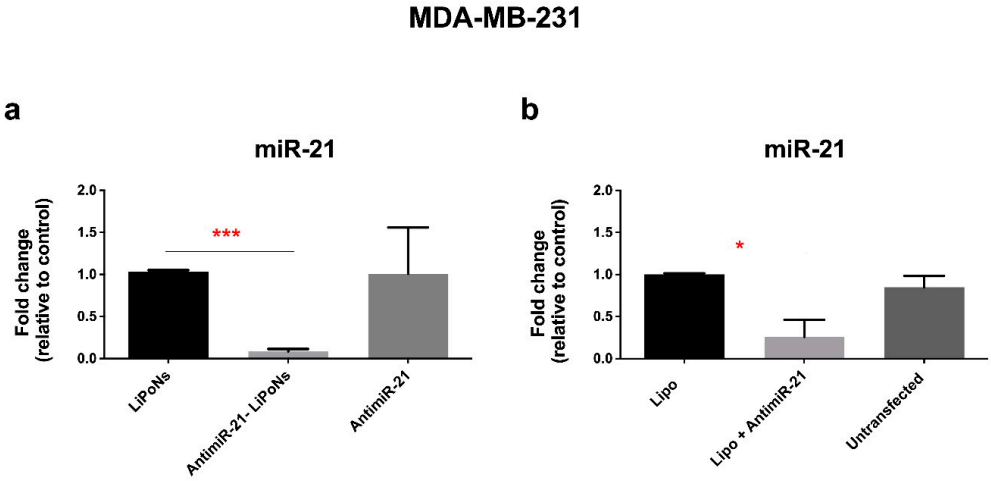

Figure 3. Efficiency of miR-21 silencing by AntimiR-21-LiPoNs in MDA-MB-231 cells. (**a**) MDA-MB-231 cells were treated with LiPoNs (used as control), AntimiR-21-LiPoNs, and AntimiR-21. (**b**) MDA-MB-231 cells were transfected with only Lipofectamine 3000 reagent (Lipo, used as a control), AntimiR-21 together with Lipofectamine 3000 (Lipo + AntimiR-21), or untransfected. After 72 h, total RNA was extracted, and the expression level of miR-21 was evaluated by q-RT-PCR. The fold change in miR-21 was calculated by normalizing the absolute levels of miR-21 to those of internal control (U6 snRNA) and setting the value of LiPoNs (**a**) and of Lipo (**b**) equal to 1. The transfections were performed three times. Bar represents the mean ± st. error of three independent experiments (* $p < 0.05$; *** $p < 0.001$).

3.3. Downstream Regulation of miR-21 Target Genes

The miR-21 targets many gene transcripts, such as phosphatase and TENsin homolog deleted on chromosome 10 (PTEN) and programmed cell death 4 (PDCD4), resulting in increased cancer cell transformation, invasion, and metastasis [67–69]. To verify the bioactivity of AntimiR-21 on the expression levels of downstream genes, the mRNA levels of miR-21 target genes were analyzed in MDA-MB-231 cells treated for 72 h with 33 nM of AntimiR-21 in the LiPoNs and Lipofectamine 3000-mediated transfection (Lipo + AntimiR-21). PTEN and PDCD4 gene levels were quantified by q-RT PCR and normalized to the housekeeping mRNA β-actin. The results show an upregulation of 4.77 times of PTEN expression for the treatment with AntimiR-21-LiPoNs (Figure 4a,b), while PDCD4 shows an upregulation of 7.3 times with respect to the control LipoNs-treated cells (Figure 4c,d).

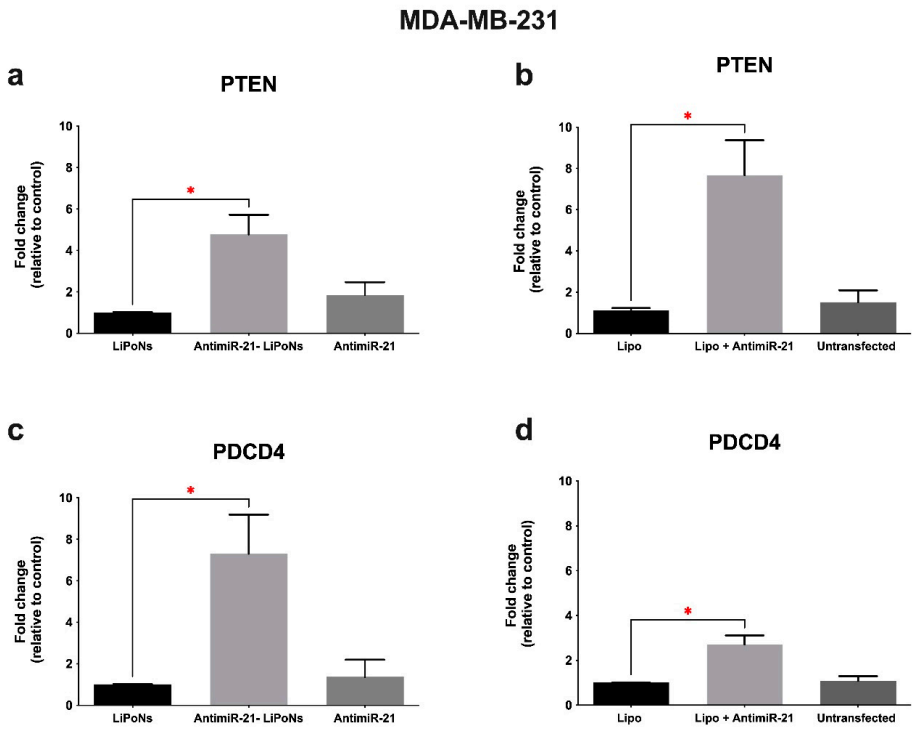

Figure 4. Efficiency of AntimiR-21-LiPoNs in downregulating the miR-21 target genes in MDA-MB-231 cells. (**a**) Expression level of PTEN mRNA was analyzed by q-RT-PCR in MDA-MB-231 cells treated for 72 h with LiPoNs, AntimiR-21-LiPoNs, or treated only with AntimiR-21. (**b**) Expression level of PTEN mRNA was analyzed by q-RT-PCR in MDA-MB-231 cells transfected for 72 h with AntimiR-21 using Lipofectamine 3000 (Lipo + AntimiR-21) or transfected only with Lipofectamine 3000 (Lipo, used as a control) or untransfected. (**c**) Expression level of PDCD4 in the cells transfected with LiPoNs, AntimiR-21-LiPoNs, or treated only with AntimiR-21. (**d**) Expression level of PDCD4 mRNA in MDA-MB-231 cell line, untransfected or transfected, for 72 h, with Lipofectamine 3000 reagent alone (Lipo) or in combination with the AntimiR-21 (Lipo + AntimiR-21). The fold change was calculated by normalizing the Ct of PTEN (**a**,**b**) and of PDCD4 (**c**,**d**) to the Ct of β-actin used as an internal control. The value of PTEN and of PDCD4 in LiPoNs (**a**–**c**) and Lipo (**b**,**d**) was set equal to 1. The transfections were performed three times, and the q-RT-PCR was performed in triplicate. Bars represent the mean ± SEM of three independent experiments (* $p < 0.05$).

As already outlined above, the AntimiR-21 entrapped in LiPoNs after 72 h of treatment confirms the activity of AntimiR-21.

No increase in either target gene is reported for free AntimiR-21, underlining the inefficient delivery of naked Antisense miRNA.

To determine whether the upregulation of PTEN and PDCD4 mRNA observed following AntimiR-21 treatment was also reflected at the protein level, a Western blot analysis was performed on MDA-MB-231 cells treated for 72 h with 33 nM AntimiR-21 delivered via LiPoNs (AntimiR-21–LiPoNs). As shown in Figure 5, AntimiR-21–LiPoN treatment induced a moderate increase in PTEN and PDCD4 protein expression compared with control cells treated with empty LiPoNs. These findings demonstrate that AntimiR-21 delivery via LiPoNs effectively restores the expression of its target genes at both transcript and protein levels.

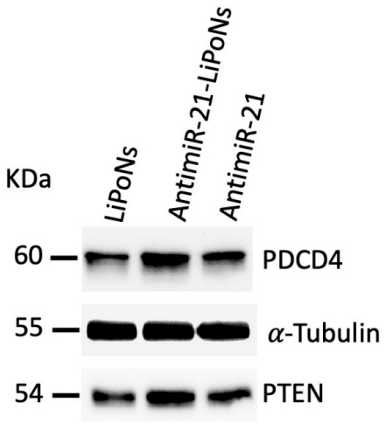

Figure 5. Expression of PTEN and PDCD4 proteins following AntimiR-21 treatment in MDA-MB-231 cells. Protein levels of PTEN and PDCD4 in cells treated with LiPoNs alone, AntimiR-21-LiPoNs, or AntimiR-21. α-tubulin was used as a loading control.

3.4. Effect on Migration Ability of MDA-MB-231 Cells by AntimiR-21-LiPoNs

miR-21 is associated with an increased migratory behavior of human breast cancer cells [65,66]. Indeed, its target genes, the PTEN and PDCD4, are related to several pathways that lead to the acquisition of invasive abilities of the cells [67,68]. Therefore, we studied the biological activity of AntimiR-21-LiPoNs, achieved through the inhibition of miR-21 with AntimiR-21, on the migration properties of MDA-MB-231 cells (Figure 6).

Thus, we silenced miR-21 in the triple-negative breast cancer MDA-MB-231 cells using the AntimiR-21-LiPoNs (Figure 6a) or those combined with Lipofectamine 3000 (Lipo + AntimiR-21) at 33 nM (Figure 6b).

In parallel, the cells were also treated with LiPoNs or Lipofectamine 3000 (Lipo) alone as controls, as in the previous cell treatments.

After 48 h from transfection, a scraped wound was introduced to the confluent monolayers, and then the migration ability was monitored by time-lapse microscopy for 24 h and expressed as a percentage of wound closure. Quantitative measurements of the wound closure at different time points showed that the silencing of miR-21 impaired the migration of MDA-MB-231 cells using both the LiPoNs as a vehicle and the Lipofectamine 3000 as a reagent.

Indeed, after 12 h, cells treated with LiPoNs presented a closure of 100%, while cells treated with AntimiR-21-LiPoNs presented a closure of 47% (Figure 6a).

Simultaneously, as reported in Figure 6b, a closure of 51.9% and of 91% was observed in cells transfected with AntimiR-21 using Lipofectamine and in cells transfected with Lipofectamine alone, respectively.

The reductions in cell migration obtained by AntimiR-21-LipoNs and Lipo + Anti miR-21 were observed at all the time points studied up to 24 h (Figure 6a,b).

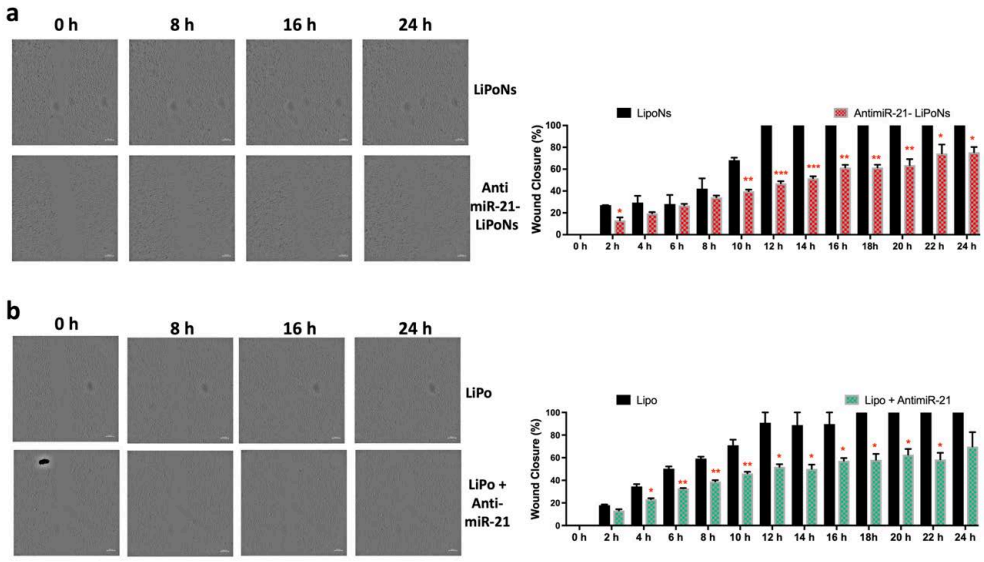

Figure 6. Effects of the AntimiR-21 delivered by LiPoNs on the migration ability of MDA-MD-231 cells. (**a**) Cells were treated with AntimiR-21-LiPoNs or LiPoNs. (**b**) Cells were transfected with the AntimiR-21 using Lipofectamine 3000 (Lipo + AntimiR-21), while cells with Lipofectamine 3000 alone (Lipo) were used as a control. (**a**,**b**). After 48 h from transfection, a scraped wound was introduced, and cell migration into the wound was recorded for 24 h using time-lapse microscopy. Wound closure was measured every two hours by calculating pixel densities in the wound area and expressed as a percentage of wound closure of triplicate areas ± st. error. * $p < 0.05$; ** $p < 0.01$; *** $p < 0.001$, unpaired *t*-test.

The good correlation between the data obtained with LiPoNs nanoparticles and the standard protocol, Lipofectamine transfection reagent, confirms the effectiveness of AntimiR-21-LiPoNs treatment in reducing the migratory properties of human breast cancer cells [70].

To test the cell viability of MDA-MB-231 cells treated with different AntimiR-21 formulations, the MTT assay was performed at 24 h and 48 h (Figure S4). Treatment with AntimiR-21 alone, in both LiPoNs formulations and mediated with Lipofectamine, produced no significant reductions in cell viability when compared with control groups, which is consistent with the results of the cytotoxicity test reported by Devulapally et al. [66] even at higher AntimiR-21 concentrations.

4. Discussion

To address the inherent instability of RNA therapeutics, diverse strategies have been implemented, including chemical modification of RNA backbones and the design of nanotechnology-based delivery systems capable of shielding RNA from nuclease-mediated degradation and improving its bioavailability in the bloodstream [20,71]. Nevertheless, post-internalization trafficking frequently leads to entrapment in endosomal or lysosomal vesicles, hindering cytosolic release and thereby reducing the biological activity of RNA payloads [19,20]. This limitation constrains their applicability in both therapeutic and theranostic settings [72].

To overcome these barriers, programmable materials have been engineered for microRNA delivery, predominantly in the form of polymer- and lipid-based nanocarrier systems [19–21,73,74]. Yet, the synergistic advantages of hybrid lipid–polymer systems, which unite the structural stability and controlled release properties of polymers with the membrane fusion capability of lipids, have not been systematically investigated.

Accordingly, hybrid nanoparticles represent a promising platform for advancing the understanding and optimization of microRNA delivery, thereby enabling precise modu-

lation of essential biological pathways. Here, we designed a core–shell structure, lipid–polymer nanoparticles (LiPoNs), co-loaded with AntimiR-21 and Gd-DTPA, where the lipid bilayer is anchored to a polymer core. Specifically, the incorporation of cholesterol and phosphatidylcholine into the carrier shell was designed to enhance cellular interactions by modulating membrane fluidity and rigidity [3,75–77]. In parallel, the chitosan core conferred enhanced stability to the AntimiR-21 molecules following internalization. Moreover, the pre-formed polymer–miRNA complex mitigated RNA degradation within the acidic endosomal environment, thereby facilitating the efficient release of intact AntimiR-21 into the cytoplasm [20,78].

As a result, the MDA-MB-231 cells transfected with the AntimiR-21-LiPoNs showed an upregulation of the gene of interest, reducing their motility. Fine control of the synthetic identity of the LiPoNs in the codelivery of active agents was obtained by coupled Hydrodynamic Flow Focusing (cHFF), previously published by our group for the encapsulation of irinotecan hydrochloride [55].

Our biological results confirm that hybrid systems, such as LiPoNs, offer stable and safe delivery of miRNA to the cells, as already obtained in other systems using nanohydrogels [79], PLGA-based nanostructures [66,80], lipid-based NPs [81–83], and core–shell supramolecular nanovectors [74] in different cancer cell lines, but moreover, they have potentially improved tunability of the release behavior and uptake mechanisms.

The strength of our strategy lies in the use of a natural polymer, chitosan, which, despite ongoing debate regarding its buffering capacity compared to other cationic polymers such as PEI [84,85], effectively facilitates endosomal/lysosomal escape due to its acidic properties. Notably, Richard et al. [85] demonstrated that the buffering capacity of chitosan is higher than that of PEI when the comparison is conducted in terms of moles. We designed the chitosan core to exploit the protonation of its amine groups under endosomal pH, triggering osmotic swelling and membrane destabilization (proton sponge effect) to facilitate endosomal escape and efficient cytosolic delivery of AntimiR-21 [77,86,87], preventing degradation within late endosomes [78,88]. These findings are consistent with other published studies on the transfection efficacy of chitosan nanoparticles [88], as well as the endosomal escape efficiency of so-called ‘Chitosomes’ [74].

This effect is not usually observed with pure lipid-based particles, such as lipoplexes, where the microRNAs remain trapped in the endosomes, unless in cases when ionizable lipids or lipids with two unsaturated chains are employed to destabilize the endosomal membrane [3,20,22].

The reported peculiar cellular behavior highlights the role that some classes of cationic polymer materials, in combination with lipids, could have in RNA-based delivery, providing additional features to the nanostructures not achievable in single-material architectures. Moreover, in this scenario of hybrid systems, other properties can be triggered and, therefore, exploited.

From a forward-looking perspective, the high tunability of hybrid architectures offers opportunities to regulate nano–bio interactions through the elastic properties of the carriers. Compared with carriers composed of a single material, lipid–polymer hybrids with non-crosslinked cores exhibit adjustable elasticity, which may significantly influence nanoparticle penetration [89,90] and intracellular delivery [91–93]. The impact on these carriers to shift from one to another of internalization pathways according to the carrier elasticity has already been documented in nanogels differing in polymer crosslinking density, even though its manifestation in lipid–polymer hybrid architectures remains largely unexplored [94,95].

5. Conclusions

In conclusion, given the inherently limited cellular uptake of negatively charged microRNAs, the coordinated regulation of target genes observed following AntimiR-21–LiPoNs treatment underscores the critical role of hybrid lipid–polymer architectures in supporting efficient delivery, even in the presence of contrast agents. The strength of this approach lies in rational material selection: lipids preserve biomimetic interactions with the cell membrane, while chitosan enhances the intracellular delivery of the RNA cargo. Altogether, this work establishes a foundation for a new library of multimaterial nanostructures, in which building blocks with complementary properties self-assemble into ordered carriers, offering synergistic advantages for microRNA delivery and theranostic applications. To further exploit the potential for clinical translation, comprehensive in vivo studies are needed to evaluate the antitumor efficacy and mechanistic effects of lipid–polymer nanoparticles encapsulating AntimiR-21, as well as other RNA-based therapeutics. Such investigations are essential to determine whether hybrid nanocarriers can simultaneously engage tumor-intrinsic signaling networks and reshape the tumor–immune microenvironment (TME), thereby achieving a coordinated and durable therapeutic response.. The overall in vivo study architecture should integrate xenograft and syngeneic tumor models, thereby reflecting a dual epistemological stance: a reductionist framework enabling controlled analysis of oncogenic signaling networks and a complementary holistic perspective capturing immune dynamics and host–tumor interactions within an intact biological system.

Supplementary Materials: The following supporting information can be downloaded at: https://www.mdpi.com/article/10.3390/bioengineering13020209/s1, Figure S1. Evaluation of AntimiR-21 stability up to 4 h: (a) at room temperature (25 °C) and 4 °C and (b) at pH of 4.3 and 2.6 by keeping constant the temperature at 25 °C. AntimiR-21 stability in the mixture CH-AcOH-Water at microfluidic process conditions: pH around 4 and at room temperature without (c) and with the addition of Gd-DTPA (d) up to 4 h. Figure S2. Size distributions of LiPoNs (a), Gd-DTPA-LiPoNs (b), AntimiR-21-LiPoNs (c) and AntimiR-21-Gd-DTPA-LiPoNs (d) as function of the mean nanoparticle concentration from the three measurements. Figure S3. Calibration curve Gd-DTPA. Gd-DTPA calibration curve (dispersed in water) for sr sequence (1/T1) and localization within the curve of LiPoNs, undiluted and diluted in water 1:1, Gd-DTPA-LiPoNs undiluted and diluted in water 1:1, AntimiR-21-LiPoNs undiluted and diluted in water 1:1, AntimiR-21-Gd-DTPA-LiPoNs undiluted and diluted in water 1:1. Figure S4. Cell viability % of MDA-MB-231 cells transfected with the AntimiR-21 alone and together with Lipofectamine 3000 reagent (AntimiR-21 conc. 33 nM), with AntimiR-21 LiPoNs and AntimiR21-Gd-DTPA LiPoNs, and LiPoNs and Gd-DTPA LiPoNs (AntimiR-21conc. 33 nM, Lipids conc. 12 µg/mL and Gd-DTPA conc.:28 µM) for (a) 24 h and (b) 48 h. Table S1. Oligonucleotide sequences used for RT–qPCR.

Author Contributions: Conceptualization, E.T. and G.S.; methodology, F.R., F.M.O., N.L., G.S. and E.T.; validation, F.R., F.M.O., N.L., G.S. and E.T.; formal analysis, F.R., F.M.O., N.L., G.S. and E.T.; investigation, F.R., F.M.O. and N.L.; resources, E.T.; data curation, F.R., F.M.O., N.L., G.S. and E.T.; writing—original draft preparation, F.R., F.M.O. and N.L.; writing—review and editing, F.R., F.M.O., N.L., G.S. and E.T.; supervision, E.T. and G.S.; project administration, E.T.; funding acquisition, E.T. All authors have read and agreed to the published version of the manuscript.

Funding: This work was supported by Ministero dell'Istruzione, dell'Università e della Ricerca, Progetti di Ricerca di Rilevante Interesse Nazionale (PRIN).

Institutional Review Board Statement: Not applicable.

Informed Consent Statement: Not applicable.

Data Availability Statement: The original contributions presented in this study are included in the article/Supplementary Material. Further inquiries can be directed to the corresponding author.

Acknowledgments: We thank the reviewers for their valuable feedback which helped improve the manuscript.

Conflicts of Interest: Authors Francesca Maria Orlandella, Neila Luciano and Giuliana Salvatore were employed by the company CEINGE-Biotecnologie Avanzate "Franco Salvatore". The remaining authors declare that the research was conducted in the absence of any commercial or financial relationships that could be construed as a potential conflict of interest.

Abbreviations

The following abbreviations are used in this manuscript:

cHFF	Coupled hydrodynamic flow-focusing
LiPoNs	Lipid–polymer nanoparticles
Gd-DTPA	Gadolinium diethylenetriamine penta-acetic acid

References

1. Let's talk about lipid nanoparticles. *Nat. Rev. Mater.* **2021**, *6*, 99. [CrossRef]
2. Thi, T.T.; Suys, E.J.; Lee, J.S.; Nguyen, D.H.; Park, K.D.; Truong, N.P. Lipid-Based Nanoparticles in the Clinic and Clinical Trials: From Cancer Nanomedicine to COVID-19 Vaccines. *Vaccines* **2021**, *9*, 359. [CrossRef] [PubMed]
3. Hou, X.; Zaks, T.; Langer, R.; Dong, Y. Lipid nanoparticles for mRNA delivery. *Nat. Rev. Mater.* **2021**, *6*, 1078–1094. [CrossRef]
4. Niu, H.; Zhao, P.; Sun, W. Biomaterials for chimeric antigen receptor T cell engineering. *Acta Biomater.* **2023**, *166*, 1–13. [CrossRef] [PubMed]
5. Long, J.; Wang, Y.; Jiang, X.; Ge, J.; Chen, M.; Zheng, B.; Wang, R.; Wang, M.; Xu, M.; Ke, Q.; et al. Nanomaterials Boost CAR-T Therapy for Solid Tumors. *Adv. Healthc. Mater.* **2024**, *13*, e2304615. [CrossRef]
6. Baden, L.R.; El Sahly, H.M.; Essink, B.; Kotloff, K.; Frey, S.; Novak, R.; Diemert, D.; Spector, S.A.; Rouphael, N.; Creech, C.B.; et al. Efficacy and Safety of the mRNA-1273 SARS-CoV-2 Vaccine. *N. Engl. J. Med.* **2021**, *384*, 403–416. [CrossRef]
7. Polack, F.; Thomas, S.J.; Kitchin, N.; Absalon, J.; Gurtman, A.; Lockhart, S.; Perez, J.L.; Pérez Marc, G.; Moreira, E.D.; Zerbini, C.; et al. Safety and Efficacy of the BNT162b2 mRNA Covid-19 Vaccine. *N. Engl. J. Med.* **2020**, *383*, 2603–2615. [CrossRef] [PubMed]
8. Billingsley, M.; Singh, N.; Ravikumar, P.; Zhang, R.; June, C.H.; Mitchell, M.J. Ionizable Lipid Nanoparticle-Mediated mRNA Delivery for Human CAR T Cell Engineering. *Nano Lett.* **2020**, *20*, 1578–1589. [CrossRef]
9. Billingsley, M.; Hamilton, A.G.; Mai, D.; Patel, S.K.; Swingle, K.L.; Sheppard, N.C.; June, C.H.; Mitchell, M.J. Orthogonal Design of Experiments for Optimization of Lipid Nanoparticles for mRNA Engineering of CAR T Cells. *Nano Lett.* **2022**, *22*, 533–542. [CrossRef]
10. Zhang, G.; Tang, T.; Chen, Y.; Huang, X.; Liang, T. mRNA vaccines in disease prevention and treatment. *Signal Transduct. Target. Ther.* **2023**, *8*, 365. [CrossRef]
11. Scheideler, M.; Vidakovic, I.; Prassl, R. Lipid nanocarriers for microRNA delivery. *Chem. Phys. Lipids* **2020**, *226*, 104837. [CrossRef]
12. Moukhtari, S.; Garbayo, E.; Amundarain, A.; Pascual-Gil, S.; Carrasco-León, A.; Prosper, F.; Agirre, X.; Blanco-Prieto, M.J. Lipid nanoparticles for siRNA delivery in cancer treatment. *J. Control. Release* **2023**, *361*, 130–146. [CrossRef]
13. Subhan, M.; Torchilin, V. Advances in siRNA Drug Delivery Strategies for Targeted TNBC Therapy. *Bioengineering* **2024**, *11*, 830. [CrossRef] [PubMed]
14. Santulli, G. Exploiting microRNA Specificity and Selectivity: Paving a Sustainable Path Towards Precision Medicine. In *Microrna: Medical Evidence: From Molecular Biology to Clinical Practice*; Springer: Cham, Germany, 2015; pp. 1–3.
15. El Sayed, S.R.; Cristante, J.; Guyon, L.; Denis, J.; Chabre, O.; Cherradi, N. MicroRNA Therapeutics in Cancer: Current Advances and Challenges. *Cancers* **2021**, *13*, 2680. [CrossRef]
16. van Zandwijk, N.; Pavlakis, N.; Kao, S.; Clarke, S.; Lee, A.; Brahmbhatt, H.; Macdiarmid, J.; Pattison, S.; Leslie, F.; Huynh, Y.; et al. Mesomir 1: A Phase I Study of Targomirs in Patients with Refractory Malignant Pleural Mesothelioma (MPM) and Lung Cancer (NSCLC). *Ann. Oncol.* **2015**, *26*, ii16–ii19. [CrossRef]
17. Kim, T.; Croce, C. MicroRNA: Trends in clinical trials of cancer diagnosis and therapy strategies. *Exp. Mol. Med.* **2023**, *55*, 1314–1321. [CrossRef]
18. Segal, M.; Slack, F.J. Challenges identifying efficacious miRNA therapeutics for cancer. *Expert Opin. Drug Discov.* **2020**, *15*, 987–992. [CrossRef] [PubMed]
19. Lee, S.W.L.; Paoletti, C.; Campisi, M.; Osaki, T.; Adriani, G.; Kamm, R.D.; Mattu, C.; Chiono, V. MicroRNA delivery through nanoparticles. *J. Control. Release* **2019**, *313*, 80–95. [CrossRef]
20. Chen, Y.; Gao, D.Y.; Huang, L. In vivo delivery of miRNAs for cancer therapy: Challenges and strategies. *Adv. Drug Deliv. Rev.* **2015**, *81*, 128–141. [CrossRef]

21. Ghafouri-Fard, S.; Shoorei, H.; Noferesti, L.; Hussen, B.M.; Moghadam, M.H.B.; Taheri, M.; Rashnoo, F. Nanoparticle-mediated delivery of microRNAs-based therapies for treatment of disorders. *Pathol. Res. Pract.* **2023**, *248*, 154667. [CrossRef]
22. Liu, S.; Liu, J.; Li, H.; Mao, K.; Wang, H.; Meng, X.; Wang, J.; Wu, C.; Chen, H.; Wang, X.; et al. An optimized ionizable cationic lipid for brain tumor-targeted siRNA delivery and glioblastoma immunotherapy. *Biomaterials* **2022**, *287*, 121645. [CrossRef]
23. Costa, B.; Boueri, B.; Oliveira, C.; Silveira, I.; Ribeiro, A.J. Lipoplexes and polyplexes as nucleic acids delivery nanosystems: The current state and future considerations. *Expert Opin. Drug Deliv.* **2022**, *19*, 577–594. [CrossRef] [PubMed]
24. Buntum, T.; Jaruseranee, N.; Khongkow, M.; Ruktanonchai, U.; Uludağ, H.; Suwantong, O. Potential of siRNA nanoparticles-loaded chitosan/silk sericin thermosensitive hydrogels as injectable therapeutics for breast cancer. *Polymer* **2025**, *338*, 129019. [CrossRef]
25. Bose, R.; Arai, Y.; Ahn, J.C.; Park, H.; Lee, S.H. Influence of cationic lipid concentration on properties of lipid-polymer hybrid nanospheres for gene delivery. *Int. J. Nanomed.* **2015**, *10*, 5367–5382.
26. Tng, D.; Song, P.; Soeartono, A.; Yang, G.; Yang, C.; Yin, F.; Tan, C.H.; Yong, K.-T.; Lin, G. Synthesis and characterization of multifunctional hybrid-polymeric nanoparticles for drug delivery and multimodal imaging of cancer. *Int. J. Nanomed.* **2015**, *10*, 5771–5786. [CrossRef]
27. Briffault, E.; Reyes, R.; Garcia-Garcia, P.; Rouco, H.; Diaz-Gomez, L.; Arnau, M.R.; Evora, C.; Diaz-Rodriguez, P.; Delgado, A. SFRP1-Silencing GapmeR-Loaded Lipid-Polymer Hybrid Nanoparticles for Bone Regeneration in Osteoporosis: Effect of Dosing and Targeting Strategy. *Int. J. Nanomed.* **2024**, *19*, 12171–12188. [CrossRef] [PubMed]
28. Ottonelli, I.; Baraldi, C.; Ruozi, B.; Vandelli, M.A.; Tosi, G.; Duskey, J.T. Advantages and challenges of polymer-lipid hybrid nanoparticles for the delivery of biotech drugs. *Nanomedicine* **2025**, *20*, 641–643. [CrossRef]
29. Hassan, A.; Ramadan, E.; Kristó, K.; Regdon, G.; Sovány, T. Lipid-Polymer Hybrid Nanoparticles as a Smart Drug Delivery System for Peptide/Protein Delivery. *Pharmaceutics* **2025**, *17*, 797. [CrossRef]
30. González-García, D.; Tapia, O.; Évora, C.; García-García, P.; Delgado, A. Conventional and microfluidic methods: Design and optimization of lipid-polymeric hybrid nanoparticles for gene therapy. *Drug Deliv. Transl. Res.* **2025**, *15*, 908–924. [CrossRef]
31. Fang, T.; Li, L.; Tariq Muhseen, Z.; Lane, L.A.; Cai, H.; Butch, C.J.; Wang, Y. Strategic Timing of Gene Silencing: Cellular Kinetics-Based Administration of siRNA for Optimized Photothermal Cancer Treatment. *Adv. Sci.* **2025**, *12*, e10802. [CrossRef] [PubMed]
32. Sun, X.; Zhang, J.; Dong, B.; Xiong, Q.; Wang, X.; Gu, Y.; Wang, Z.; Liu, H.; Zhang, J.; He, X.; et al. Targeting SLITRK4 Restrains Proliferation and Liver Metastasis in Colorectal Cancer via Regulating PI3K/AKT/NFκB Pathway and Tumor-Associated Macrophage. *Adv. Sci.* **2024**, *12*, e2400367. [CrossRef] [PubMed]
33. Das, R.; Halabi, E.A.; Fredrich, I.R.; Oh, J.; Peterson, H.M.; Ge, X.; Scott, E.; Kohler, R.H.; Garris, C.S.; Weissleder, R. Hybrid LNP Prime Dendritic Cells for Nucleotide Delivery. *Adv. Sci.* **2023**, *10*, e2303576. [CrossRef]
34. Zhang, X.; He, Z.; Li, F.; Shan, Q.; Sun, L.; Cao, X.; Liu, Y.; Hang, Y.; Xu, Z. A Polymer-Lipid Nanosystem Comprising siRNA and Gemcitabine for Pancreatic Cancer Treatment. *Acs Appl. Nano Mater.* **2025**, *8*, 10326–10339. [CrossRef]
35. Shah, R.; Spektor, T.M.; Weisenberger, D.J.; Ding, H.; Patil, R.; Amador, C.; Song, X.-Y.; Chun, S.T.; Inzalaco, J.; Turjman, S.; et al. Reversal of dual epigenetic repression of non-canonical Wnt-5a normalises diabetic corneal epithelial wound healing and stem cells. *Diabetologia* **2023**, *66*, 1943–1958. [CrossRef]
36. Gameiro, M.; Mano, J.; Gaspar, V. Emerging lipid-polymer hybrid nanoparticles for genome editing. *Polym. Chem.* **2024**, *15*, 3436–3468. [CrossRef]
37. Pandey, P.; Arya, D.K.; Deepak, P.; Ali, D.; Alarifi, S.; Srivastava, S.; Lavasanifar, A.; Rajinikanth, P.S. αvβ3 Integrin and Folate-Targeted pH-Sensitive Liposomes with Dual Ligand Modification for Metastatic Breast Cancer Treatment. *Bioengineering* **2024**, *11*, 800. [CrossRef]
38. Su, X.F.; Fricke, J.; Kavanagh, D.G.; Irvine, D.J. In Vitro and in Vivo mRNA Delivery Using Lipid-Enveloped pH-Responsive Polymer Nanoparticles. *Mol. Pharm.* **2011**, *8*, 774–787. [CrossRef]
39. Yang, J.N.; Arya, S.; Lung, P.; Lin, Q.; Huang, J.; Li, Q. Hybrid nanovaccine for the co-delivery of the mRNA antigen and adjuvant. *Nanoscale* **2019**, *11*, 21782–21789. [CrossRef]
40. Kliesch, L.; Delandre, S.; Gabelmann, A.; Koch, M.; Schulze, K.; Guzmán, C.A.; Loretz, B.; Lehr, C.-M. Lipid-Polymer Hybrid Nanoparticles for mRNA Delivery to Dendritic Cells: Impact of Lipid Composition on Performance in Different Media. *Pharmaceutics* **2022**, *14*, 2675. [CrossRef] [PubMed]
41. Huang, X.M.; Schwind, S.; Yu, B.; Santhanam, R.; Wang, H.; Hoellerbauer, P.; Mims, A.; Klisovic, R.; Walker, A.R.; Chan, K.K.; et al. Targeted Delivery of microRNA-29b by Transferrin-Conjugated Anionic Lipopolyplex Nanoparticles: A Novel Therapeutic Strategy in Acute Myeloid Leukemia. *Clin. Cancer Res.* **2013**, *19*, 2355–2367. [CrossRef]
42. Shi, J.J.; Xu, Y.; Xu, X.; Zhu, X.; Pridgen, E.; Wu, J.; Votruba, A.R.; Swami, A.; Zetter, B.R.; Farokhzad, O.C. Hybrid lipid-polymer nanoparticles for sustained siRNA delivery and gene silencing. *Nanomed.-Nanotechnol. Biol. Med.* **2014**, *10*, 897–900.

43. Küçüktürkmen, B.; Devrim, B.; Saka, O.M.; Yilmaz, Ş.; Arsoy, T.; Bozkir, A. Co-delivery of pemetrexed and miR-21 antisense oligonucleotide by lipid-polymer hybrid nanoparticles and effects on glioblastoma cells. *Drug Dev. Ind. Pharm.* **2017**, *43*, 12–21. [CrossRef] [PubMed]
44. Ali, M.; Hooshmand, N.; El-Sayed, M.; Labouta, H.I. Microfluidics for Development of Lipid Nanoparticles: Paving the Way for Nucleic Acids to the Clinic. *Acs Appl. Bio Mater.* **2021**, *6*, 3566–3576. [CrossRef]
45. Shepherd, S.J.; Issadore, D.; Mitchell, M.J. Microfluidic formulation of nanoparticles for biomedical applications. *Biomaterials* **2021**, *274*, 120826. [CrossRef]
46. Cheng, Y.; Hay, C.D.; Mahuttanatan, S.M.; Hindley, J.W.; Ces, O.; Elani, Y. Microfluidic technologies for lipid vesicle generation. *Lab A Chip* **2024**, *24*, 4679–4716. [CrossRef]
47. Maeki, M.; Uno, S.; Niwa, A.; Okada, Y.; Tokeshi, M. Microfluidic technologies and devices for lipid nanoparticle-based RNA delivery. *J. Control. Release* **2022**, *344*, 80–96. [CrossRef] [PubMed]
48. Leung, A.; Tam, Y.Y.C.; Chen, S.; Hafez, I.M.; Cullis, P.R. Microfluidic Mixing: A General Method for Encapsulating Macromolecules in Lipid Nanoparticle Systems. *J. Phys. Chem. B* **2015**, *119*, 8698–8706. [CrossRef] [PubMed]
49. Shepherd, S.; Warzecha, C.C.; Yadavali, S.; El-Mayta, R.; Alameh, M.-G.; Wang, L.; Weissman, D.; Wilson, J.M.; Issadore, D.; Mitchell, M.J. Scalable mRNA and siRNA Lipid Nanoparticle Production Using a Parallelized Microfluidic Device. *Nano Lett.* **2021**, *21*, 5671–5680. [CrossRef]
50. Balbino, T.; Serafin, J.M.; Radaic, A.; de Jesus, M.B.; de la Torre, L.G. Integrated microfluidic devices for the synthesis of nanoscale liposomes and lipoplexes. *Colloids Surf. B-Biointerfaces* **2017**, *152*, 406–413. [CrossRef]
51. Chen, D.L.; Love, K.T.; Chen, Y.; Eltoukhy, A.A.; Kastrup, C.; Sahay, G.; Jeon, A.; Dong, Y.; Whitehead, K.A.; Anderson, D.G. Rapid Discovery of Potent siRNA-Containing Lipid Nanoparticles Enabled by Controlled Microfluidic Formulation. *J. Am. Chem. Soc.* **2012**, *134*, 6948–6951.
52. Belliveau, N.M.; Huft, J.; Lin, P.J.; Chen, S.; Leung, A.K.; Leaver, T.J.; Wild, A.W.; Lee, J.B.; Taylor, R.J.; Tam, Y.K.; et al. Microfluidic Synthesis of Highly Potent Limit-size Lipid Nanoparticles for In Vivo Delivery of siRNA. *Mol. Ther.-Nucleic Acids* **2012**, *1*, e37.
53. Russo, M.; Bevilacqua, P.; Netti, P.A.; Torino, E. A Microfluidic Platform to design crosslinked Hyaluronic Acid Nanoparticles (cHANPs) for enhanced MRI. *Sci. Rep.* **2016**, *6*, 37906. [CrossRef]
54. Costagliola di Polidoro, A.; Zambito, G.; Haeck, J.; Mezzanotte, L.; Lamfers, M.; Netti, P.A.; Torino, E. Theranostic Design of Angiopep-2 Conjugated Hyaluronic Acid Nanoparticles (Thera-ANG-cHANPs) for Dual Targeting and Boosted Imaging of Glioma Cells. *Cancers* **2021**, *13*, 503. [CrossRef]
55. Roffo, F.; Ponsiglione, A.M.; Netti, P.A.; Torino, E. coupled Hydrodynamic Flow Focusing (cHFF) to Engineer Lipid-Polymer Nanoparticles (LiPoNs) for Multimodal Imaging and Theranostic Applications. *Biomedicines* **2022**, *10*, 438. [CrossRef]
56. Smeraldo, A.; Ponsiglione, A.M.; Netti, P.A.; Torino, E. Tuning of Hydrogel Architectures by Ionotropic Gelation in Microfluidics: Beyond Batch Processing to Multimodal Diagnostics. *Biomedicines* **2021**, *9*, 1551. [CrossRef] [PubMed]
57. Zhao, W.Y.; Zhang, C.; Li, B.; Zhang, X.; Luo, X.; Zeng, C.; Li, W.; Gao, M.; Dong, Y. Lipid Polymer Hybrid Nanomaterials for mRNA Delivery. *Cell. Mol. Bioeng.* **2018**, *11*, 397–406. [CrossRef] [PubMed]
58. Meyer, R.A.; Hussmann, G.P.; Peterson, N.C.; Santos, J.L.; Tuesca, A.D. A scalable and robust cationic lipid/polymer hybrid nanoparticle platform for mRNA delivery. *Int. J. Pharm.* **2022**, *611*, 121314. [PubMed]
59. Santhanes, D.; Wilkins, A.; Zhang, H.; Aitken, R.J.; Liang, M. Microfluidic formulation of lipid/polymer hybrid nanoparticles for plasmid DNA (pDNA) delivery. *Int. J. Pharm.* **2022**, *627*, 122223.
60. Wei, W.; Sun, J.; Guo, X.-Y.; Chen, X.; Wang, R.; Qiu, C.; Zhang, H.-T.; Pang, W.-H.; Wang, J.-C.; Zhang, Q. Microfluidic-Based Holonomic Constraints of siRNA in the Kernel of Lipid/Polymer Hybrid Nanoassemblies for Improving Stable and Safe In Vivo Delivery. *Acs Appl. Mater. Interfaces* **2020**, *12*, 14839–14854. [CrossRef]
61. Alawi, M.; Hilles, A.R.; Kumar, M.; Ansari, M.D.; Mahmood, S. Lipid-polymer hybrid nanoparticles: A cutting-edge frontier in breast cancer treatment strategies. *Nanomedicine* **2025**, *20*, 1775–1798.
62. Orlandella, F.; Mirabelli, P.; De Stefano, A.E.; Iervolino, P.L.C.; Luciano, N.; D'Angelo, S.; Salvatore, G. Effects of Annurca Flesh Apple Polyphenols in Human Thyroid Cancer Cell Lines. *Oxidative Med. Cell. Longev.* **2022**, *2022*, 6268755. [CrossRef]
63. Pogocki, D.; Schöneich, C. Chemical stability of nucleic acid-derived drugs. *J. Pharm. Sci.* **2000**, *89*, 443–456. [CrossRef]
64. Goldman, M.; Craft, B.; Hastie, M.; Repečka, K.; McDade, F.; Kamath, A.; Banerjee, A.; Luo, Y.; Rogers, D.; Brooks, A.N.; et al. Visualizing and interpreting cancer genomics data via the Xena platform. *Nat. Biotechnol.* **2020**, *38*, 675–678. [CrossRef] [PubMed]
65. Arisan, E.; Rencuzogullari, O.; Cieza-Borrella, C.; Arenas, F.M.; Dwek, M.; Lange, S.; Uysal-Onganer, P. MiR-21 Is Required for the Epithelial-Mesenchymal Transition in MDA-MB-231 Breast Cancer Cells. *Int. J. Mol. Sci.* **2021**, *22*, 1557. [CrossRef]
66. Devulapally, R.; Sekar, N.M.; Sekar, T.V.; Foygel, K.; Massoud, T.F.; Willmann, J.K.; Paulmurugan, R. Polymer Nanoparticles Mediated Codelivery of AntimiR-10b and AntimiR-21 for Achieving Triple Negative Breast Cancer Therapy. *Acs Nano* **2015**, *9*, 2290–2302. [CrossRef]
67. Bermúdez Brito, M.; Goulielmaki, E.; Papakonstanti, E.A. Focus on PTEN Regulation. *Front. Oncol.* **2015**, *5*, 166. [CrossRef]

68. Matsuhashi, S.; Manirujjaman, M.; Hamajima, H.; Ozaki, I. Control Mechanisms of the Tumor Suppressor PDCD4: Expression and Functions. *Int. J. Mol. Sci.* **2019**, *20*, 2304. [CrossRef]
69. Ghosh, A.; Ranjan, N.; Jiang, L.; Ansari, A.H.; Degyatoreva, N.; Ahluwalia, S.; Arya, D.P.; Maiti, S. Fine-tuning miR-21 expression and inhibition of EMT in breast cancer cells using aromatic-neomycin derivatives. *Mol. Ther.-Nucleic Acids* **2022**, *27*, 685–698. [CrossRef] [PubMed]
70. Davis, S.; Lollo, B.; Freier, S.; Esau, C. Improved targeting of miRNA with antisense oligonucleotides. *Nucleic Acids Res.* **2006**, *34*, 2294–2304. [CrossRef]
71. Fu, Y.; Chen, J.; Huang, Z. Recent progress in microRNA-based delivery systems for the treatment of human disease. *ExRNA* **2019**, *1*, 24. [CrossRef]
72. Yasir, M.; Mishra, R.; Tripathi, A.S.; Maurya, R.K.; Shahi, A.; Zaki, M.E.A.; Al Hussain, S.A.; Masand, V.H. Theranostics: A multifaceted approach utilizing nano-biomaterials. *Discover Nano* **2024**, *19*, 35. [CrossRef] [PubMed]
73. Wang, C.; Zhang, Y.; Kong, W.; Rong, X.; Zhong, Z.; Jiang, L.; Chen, S.; Li, C.; Zhang, F.; Jiang, J. Delivery of miRNAs Using Nanoparticles for the Treatment of Osteosarcoma. *Int. J. Nanomed.* **2024**, *19*, 8641–8660. [CrossRef] [PubMed]
74. Sun, X.F.; Xu, H.; Huang, T.; Zhang, C.; Wu, J.; Luo, S. Simultaneous delivery of anti-miRNA and docetaxel with supramolecular self-assembled "chitosome" for improving chemosensitivity of triple negative breast cancer cells. *Drug Deliv. Transl. Res.* **2021**, *11*, 192–204. [CrossRef]
75. Vencken, S.; Foged, C.; Ramsey, J.M.; Sweeney, L.; Cryan, S.-A.; MacLoughlin, R.J.; Greene, C.M. Nebulised lipid-polymer hybrid nanoparticles for the delivery of a therapeutic anti-inflammatory microRNA to bronchial epithelial cells. *Erj Open Res.* **2019**, *5*, 00161-2018. [CrossRef]
76. Patel, S.; Ashwanikumar, N.; Robinson, E.; Xia, Y.; Mihai, C.; Griffith, J.P., III; Hou, S.; Esposito, A.A.; Ketova, T.; Welsher, K.; et al. Naturally-occurring cholesterol analogues in lipid nanoparticles induce polymorphic shape and enhance intracellular delivery of mRNA. *Nat. Commun.* **2020**, *11*, 983.
77. Parodi, A.; Corbo, C.; Cevenini, A.; Molinaro, R.; Palomba, R.; Pandolfi, L.; Agostini, M.; Salvatore, F.; Tasciotti, E. Enabling cytoplasmic delivery and organelle targeting by surface modification of nanocarriers. *Nanomedicine* **2015**, *10*, 1923–1940. [CrossRef]
78. Cao, Y.; Tan, Y.F.; Wong, Y.S.; Liew, M.W.J.; Venkatraman, S. Recent Advances in Chitosan-Based Carriers for Gene Delivery. *Mar. Drugs* **2019**, *17*, 381. [CrossRef]
79. Javanmardi, S.; Abolmaali, S.S.; Mehrabanpour, M.J.; Aghamaali, M.R.; Tamaddon, A.M. PEGylated nanohydrogels delivering anti-MicroRNA-21 suppress ovarian tumor-associated angiogenesis in matrigel and chicken chorioallantoic membrane models. *Bioimpacts* **2022**, *12*, 449–461. [CrossRef] [PubMed]
80. Devulapally, R.; Sekar, T.V.; Paulmurugan, R. Formulation of Anti-miR-21 and 4-Hydroxytamoxifen Co-loaded Biodegradable Polymer Nanoparticles and Their Antiproliferative Effect on Breast Cancer Cells. *Mol. Pharm.* **2015**, *12*, 2080–2092. [CrossRef]
81. Li, J.; Ma, Q.; Zhang, X.; Chen, X.; Lin, J.; Bai, J.; Su, F.; Zhao, X.; Lee, R.J.; Yang, Y. Antitumor activity of lipid nanoparticle-delivered anti-miR-21. *Mol. Cancer Ther.* **2023**, *22*, A174. [CrossRef]
82. Yan, L.; Su, Y.; Hsia, I.; Xu, Y.; Vincent-Chong, V.K.; Mojica, W.; Seshadri, M.; Zhao, R.; Wu, Y. Delivery of anti-microRNA-21 by lung-targeted liposomes for pulmonary fibrosis treatment. *Mol. Ther.-Nucleic Acids* **2023**, *32*, 36–47.
83. Zhang, Z.; Huang, Y.; Li, J.; Su, F.; Kuo, J.C.; Hu, Y.; Zhao, X.; Lee, R.J. Antitumor Activity of Anti-miR-21 Delivered through Lipid Nanoparticles. *Adv. Heal. Mater.* **2023**, *12*, e2202412. [CrossRef] [PubMed]
84. Mao, H.; Roy, K.; Troung-Le, V.L.; Janes, K.A.; Lin, K.Y.; Wang, Y.; August, J.; Leong, K.W. Chitosan-DNA nanoparticles as gene carriers: Synthesis, characterization and transfection efficiency. *J. Control. Release* **2001**, *70*, 399–421. [CrossRef] [PubMed]
85. Richard, I.; Thibault, M.; De Crescenzo, G.; Buschmann, M.D.; Lavertu, M. Ionization Behavior of Chitosan and Chitosan-DNA Polyplexes Indicate That Chitosan Has a Similar Capability to Induce a Proton-Sponge Effect as PEI. *Biomacromolecules* **2013**, *14*, 1732–1740. [CrossRef]
86. Ishii, T.; Okahata, Y.; Sato, T. Mechanism of cell transfection with plasmid/chitosan complexes. *Biochim. Biophys. Acta (BBA)-Biomembr.* **2001**, *1514*, 51–64. [CrossRef]
87. Köping-Höggård, M.; Tubulekas, I.; Guan, H.; Edwards, K.; Nilsson, M.; Vårum, K.; Artursson, P. Chitosan as a nonviral gene delivery system. Structure-property relationships and characteristics compared with polyethylenimine in vitro and after lung administration in vivo. *Gene Ther.* **2001**, *8*, 1108–1121. [CrossRef]
88. Antoniou, V.; Mourelatou, E.A.; Galatou, E.; Avgoustakis, K.; Hatziantoniou, S. Gene Therapy with Chitosan Nanoparticles: Modern Formulation Strategies for Enhancing Cancer Cell Transfection. *Pharmaceutics* **2024**, *16*, 868. [CrossRef] [PubMed]
89. Gao, Y.; Li, M.; Chen, B.; Shen, Z.; Guo, P.; Wientjes, M.G.; Au, J.L.-S. Predictive Models of Diffusive Nanoparticle Transport in 3-Dimensional Tumor Cell Spheroids. *Aaps J.* **2013**, *15*, 816–831. [CrossRef]
90. Wientjes, M.G.; Yeung, B.Z.; Lu, Z.; Wientjes, M.G.; Au, J.L. Predicting diffusive transport of cationic liposomes in 3-dimensional tumor spheroids. *J. Control. Release* **2014**, *192*, 10–18. [CrossRef]
91. Hui, Y.; Yi, X.; Hou, F.; Wibowo, D.; Zhang, F.; Zhao, D.; Gao, H.; Zhao, C.-X. Role of Nanoparticle Mechanical Properties in Cancer Drug Delivery. *Acs Nano* **2019**, *13*, 7410–7424. [CrossRef]

92. Anselmo, A.C.; Mitragotri, S. Nanoparticles in the clinic: An update post COVID-19 vaccines. *Bioeng. Transl. Med.* **2021**, *6*, e10246. [CrossRef] [PubMed]
93. Bompard, J.; Rosso, A.; Brizuela, L.; Mebarek, S.; Blum, L.J.; Trunfio-Sfarghiu, A.-M.; Lollo, G.; Granjon, T.; Girard-Egrot, A.; Maniti, O. Membrane Fluidity as a New Means to Selectively Target Cancer Cells with Fusogenic Lipid Carriers. *Langmuir* **2020**, *36*, 5134–5144. [CrossRef] [PubMed]
94. Guo, P.; Liu, D.; Subramanyam, K.; Wang, B.; Yang, J.; Huang, J.; Auguste, D.T.; Moses, M.A. Nanoparticle elasticity directs tumor uptake. *Nat. Commun.* **2018**, *9*, 130. [CrossRef]
95. Kim, J.; Eygeris, Y.; Gupta, M.; Sahay, G. Self-assembled mRNA vaccines. *Adv. Drug Deliv. Rev.* **2021**, *170*, 83–112. [CrossRef] [PubMed]